DOI:10.22337/2587-9618-2020-16-2-26-38

HIGH-THROUGHPUT DEEP LEARNING ALGORITHM FOR DIAGNOSIS AND DEFECTS CLASSIFICATION OF WATERPROOFING MEMBRANES

Darya Filatova[1,2], Charles El-Nouty[3], Uladzislau Punko[2]
[1]CHArt, EPHE, Paris, FRANCE
[2]Faculty of Computer Systems and Networks Belarusian State University of Informatics and Radioelectronics, Minsk, BELARUS
[3] LAGA, UMR 7539, F-93430, Université Sorbonne Paris Nord, Paris, FRANCE

Abstract: The work is devoted to the development of a high-performance deep learning algorithm related to the diagnosis and classification of defects of water-repellent membranes. The mechanism of constructing visual models of the membrane surface is discussed. This allows to get the representative training data set. The proposed methodology consists in the sequent transformations of pixel-image intensities to find defected fragments on the membrane's surface. The computational algorithm is based on the architecture of convolution neural networks. To assess its effectiveness, the "confidence of confidence" criterion is proposed. The presented computations show that the methodology can be successfully applied in material sciences, for example, to study the properties of building materials, or in forensic science when examining the causes of construction catastrophes.

Keywords*:* waterproofing membranes, deep learning, machine learning, pathology classification

ВЫСОКОПРОИЗВОДИТЕЛЬНЫЙ АЛГОРИТМ ГЛУБОКОГО ОБУЧЕНИЯ ДЛЯ ДИАГНОСТИКИ И КЛАССИФИКАЦИИ ДЕФЕКТОВ ВОДООТТАЛКИВАЮЩИХ МЕМБРАН

Дарья Филатова[1,2], Шарль Эль-Нути[3], Владислав Пунько
[1] Лаборатория Человеческого и Искусственного Познания
Практическая Школа Высших Исследований, Париж, ФРАНЦИЯ
[2]Факультет Компьютерных Систем и Сетей, Белорусский Государственный Университет Информатики и Радиоэлектроники, Минск, БЕЛАРУСЬ
[3] ЛАГА, СНРС, УМР 7539, Ф-93430, Университет Сорбонна Париж Север, Париж, ФРАНЦИЯ

Аннотация: Работа посвящена разработке высокопроизводительного алгоритма глубокого обучения, связанного с диагностикой и классификации дефектов водоотталкивающих мембран. Обсужден механизм построения визуальных моделей поверхности мембран, позволяющий представить эволюцию различных повреждений. Этот подход позволяет получить тренеровочный набор изображений с известным количеством дефектов. Предложенная методология основана на последовательных преобразованиях интенсивности пиксельных изображений для обнаружения дефектных фрагментов на поверхности мембраны. Вычислительный алгоритм основан на архитектуре сверточных нейронных сетей. Для оценки его эффективности предложен критерий «доверительная область». Представленные вычислителения показывают, что методологияя может быть успешно применена в материаловединии, на пример, для исследования свойств строительных материалов, или в криминологии, на пример, при изучении причин строительных катастроф.

Ключевые слова: гидроизоляционные мембраны, глубокое обучение, машинное обучение, классификация патологий

1. INTRODUCTION

The design of buildings and constructions requires an understanding of the principle of stability, durability, and rigidity of the main constructed structures. Besides, the provision of measures of the building maintenance and monitoring their technical conditions are essen-

tial during the design stage. The over-end decade of technological progress acceleration has led to the emergence of new building unique properties materials, which, on the one hand, drove to a simplification of building technologies. On the other hand, it took more stringent requirements on resistance, reliability, durability of structures [1]. The principles of building structures are changing. Virtual modeling has led to an increase in the number of available solutions to the same problems. This fact casts doubt on the authenticity of the standard design principles, thereby facilitating the selection of the right material and the development of the correct structures. Besides, the desire to find the optimal simplification of the structure without reduction of safety mostly through choosing solid materials plays an important role. For example, through chemical reactions, the hydro protective layer mechanically connects to the monolithic reinforced concrete mainstay's surface [2]. This process leads to excellent hydro isolation. Therefore, waterproofing systems perfectly work. However, such a constructive solution loses effectiveness if damage occurs. Numerous works devoted to studying the properties of composite materials often indicate that mechanical damage to the membrane insulation leads to lateral migration of water inside the structure [1–3]. That means the place of soaking does not always match the location of insulation's damage, which unpredictably changes the structure's technical parameters. These papers indicated that the study of the phenomenon of water migration using new technologies and materials requires a new experimental research methodology to identify and classify possible pathologies in waterproofing layers [4, 5]. The solution to this problem will help designers in their subsequent work.

Civil engineering, like all other industries, is gone through the fourth industrial revolution. The main idea of this revolution consists in creating cyber-physical systems. These include physical objects and information models. The physical object is managed at every life cycle stage (from the project concept to the moment of decommissioning) using an information system that analyzes the flows of heterogeneous information using computer systems. Artificial intelligence (AI), as well as machine learning (ML), and deep learning (DL), becomes the leading information technology and not only due to the possibility to work better and faster with large amounts of information. For example, artificial intelligence algorithms simulate the work of the human brain. These last can find and classify a defect or pathology hidden from the human eyes even at an early stage of the corruption process, improving feedback on building information modeling (BIM) and thereby ensuring uninterrupted operation of the entire project.

By analogy with the task of pattern recognition applied to fault detection, this work aims to develop a methodology and an algorithm capable of identifying and classifying the visible defects on the surface of the waterproofing membranes based on available information. To promote defects detection methodology, we will use artificially generated images, imitating real photographs of some waterproofing membranes. We focus our attention on the detailed description of the AI algorithm and its quality performance. The main advantage of this approach is the scenarios' development to investigate defects' propagation on the membrane surface. The same methodology is also useful for concrete's petrographic analysis, biological materials [6].

The rest of this paper is organized in the following manner. In Section 2, we propose a brief description of waterproof membranes and detail a generalized visual model of their surface. Section 3 describes the methodology for the damages detection and classification. Next, in Section 4, we illustrate the methodology by simulation experiments. Finally, in Section 5, we give the concluding remarks concerning the methodology implementation and its further development.

2. PROBLEM FORMULATION

2.1. Conception of waterproof membranes

A waterproofing membrane is a continuous thin layer of waterproof material that is laid on some surface and which does not allow water to pass

through it. For example, if a waterproofing membrane is laid on a flat terrace between a structural slab and a finishing tile, water will no longer seep into the structural slab [4]. However, in order for this property to be maintained as long as possible, the structural surface and tile must be correctly installed. Any water that remains as puddles on the tile can leak into the plate over time, provoking corrosion of the hydro-repellent membrane, and then the structural slab. There are two types of the waterproofing membranes. Liquid–applied (see Fig. 1 and Fig. 2) and sheet–based (see Fig. 3) membranes are composed of thin about 2 to 4mm thick layers of waterproof material. Membranes can be used in different elements of a construction, namely for underneath and around basements, over terrace slabs and balconies, over landscaped concrete decks, between the soil and concrete in gutters, and many others.

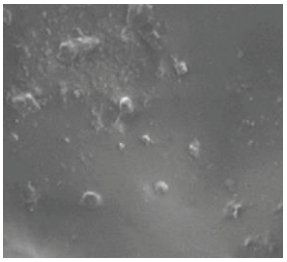

Figure 1. Some corrupted liquid–applied waterproofing membrane: pore deformation and erosive swellings

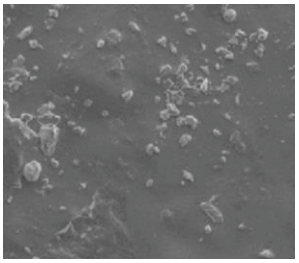

Figure 2. Some corrupted liquid–applied waterproofing membrane: erosive swellings and micro-cracks

UV stability, elongation, breathability, tear and abrasion resistances, chemical stability, geometry play an important role while selecting membrane solutions for the construction. It is impossible not to take into account the influence of the environment in which the structure will be operated. As one can imagine, over time, the desired qualities are lost. Thus, exposure to the sun and precipitation adversely affect breathability. The pores, with which the membrane breathes, over time deform and stop working. In places of deformation there are swellings and cracks. The protective property is lost leading sooner or later to the threat of structural destruction.

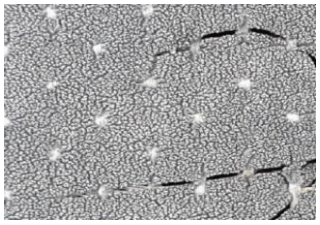

Figure 3. Some corrupted sheet–based waterproofing membrane: pore deformation and macrocracks

2.2. Generalized visual model of surface

We suppose that $n-by-m$ pixels grayscale digital image $\mathcal{I}$ corresponds to the membrane's surface associated with the bounded closed set

$$\mathcal{D}=\left[0,n-1\right]\times\left[0,m-1\right]\subset\mathbb{R}_+^2. \qquad (1)$$

For the simplicity each pixel correspond to "the smallest unit" of the membrane surface and is denoted as $(x,y)\in\mathcal{D}$. We call this unit "***a region***", that is to say, the membrane consists of the regions. Moreover, each pair $(x,y)\in\mathcal{D}$ is characterized by an intensity

$$f_{(x,y)}\in\mathcal{F},$$

where $\mathcal{F}=\{f_{\min},...,f_{\max}\}\subset\mathbb{R}_+$ is an ordered final set. The set $\mathcal{D}$ is discretized as a regular grid such that each vertex (node) has coordinates $(i\Delta x, j\Delta y)$, where Δx and Δy correspond to the grid spacing, $i\in\{1,..,n_x\}$ and $j\in\{1,..,n_y\}$ with $n_x<<n$ and $n_y<<m$. The

quantity of vertices is $n_x \times n_y$. Let us introduce the set $\mathcal{L} = \{1,..,n_x \times n_y\}$. For the simplicity we denote these coordinates as (x_i, y_j). We assume that at some instant of time t, $t \in [t_0, t_1]$, each pore $-\mathcal{R}_\ell(t)$, $\ell \in \mathcal{L}$ – of the membrane is presented by the disc of center (x_i, y_j), that is

$$\mathcal{R}_\ell(t) = \{(x,y) \in \mathcal{D} \,|\, (x - x_i)^2 + (y - y_j)^2 \le r_\ell^2(t)\}, \quad (2)$$

where $r_\ell(t)$ is the radius of the pore, $r_\ell(t_0) = r_0$. Moreover, we assume that at time t_0 that

$$\forall \ell \in \mathcal{L},\ \forall k \in \mathcal{L},\ \ell \neq k \ \Rightarrow \mathcal{R}_\ell(t_0) \cap \mathcal{R}_k(t_0) = \varnothing.$$

We denote the set of the pores by Ω. An example of the possible configuration of the surface of the membrane is illustrated by Fig. 4.

Figure 4. The visual idealized model of the membrane surface: initial state at t_0

The over-time erosion as well as the evolutionary process leading to damage to the pore, and therefore of the membrane surface at the observation time interval $[t_0, t_1]$, is associated with the change in the radius $r_\ell(t)$ of the ℓ^{th} pore, $\ell \in \mathcal{L}$, with the formation of microcracks at its edges, and with cracks propagation on the surface. We can observe these processes only as the changes of the intensities of pixels.

To model these processes we assume that at time t each pore contains $\lambda_\ell(t)$ regions included in $\mathcal{R}_\ell(t)$ and denoted as $\kappa_{\ell i}(t)$, $i \in \{1,2,...,\lambda_\ell(t)\}$. Each region is characterized by a state s, which takes one of the two values: s_0 – non-damaged state, s_1 – damaged state. The change of the state corresponds to the change of the intensities of pixels, which make corruption visible on the image. Hence, we can form the time-varying sets of all non-damaged regions

$$\mathcal{S}_{0\ell}(t) = \{\kappa_{\ell i}(t) \in \mathcal{R}_\ell(t) \,|\, s = s_0\} \quad (3)$$

and of all damaged regions

$$\mathcal{S}_{1\ell}(t) = \{\kappa_{\ell i}(t) \in \mathcal{R}_\ell(t) \,|\, s = s_1\}. \quad (4)$$

We obviously have $\mathcal{S}_{0\ell}(t) \cap \mathcal{S}_{1\ell}(t) = \varnothing$, $\mathcal{S}_{0\ell}(t) \cup \mathcal{S}_{1\ell}(t) = \mathcal{R}_\ell(t)$ for any $t \in (t_0, t_1]$. Note, that initially all the regions are in non-damaged state, i.e. $\mathcal{S}_{0\ell}(t) = \mathcal{R}_\ell(t)$. Once the radius of the pore was changed, the state of the ℓ^{th} region can be changed with some probability $p(t)$, $0 \le p(t) \le 1$, namely for $\ell \in \mathcal{L}$

$$\mathbb{P}(s_1 \leftarrow s_0 \,|\, r_\ell(t) > r_0) = p,\ t \in (t_0, t_1]. \quad (5)$$

The damaged regions form the edge-inward micro-cracks on the surface of the pore (see Fig. 5). The visual changes on the pore surface will be displayed in a darker shade of gray than the original. The membrane's surface crack propagation (see Fig. 6a) starts if there exists one pore with damaged area such that

$$\max_{\ell \in \mathcal{L}} card(\mathcal{S}_{1\ell}(t)) \ge \tilde{p}, \quad (6)$$

where $\tilde{p}$ is a critical damage level, which has to be properly chosen. The crack starts from this pore (see Fig. 6b). Here, the visual changes on

the membrane's surface will be displayed in a lighter shade of gray than the original. To model the micro-cracks the surface cracks we will use the modified algorithms of Mersenne twister pseudorandom number generator and non-uniform fractals [**7**]. Finally, to model the non-uniform background of the membrane the fractional Brownian fields [8, 9] with different values of Hurst parameters $H \in (0,1)$ are be used (see Fig. 7).

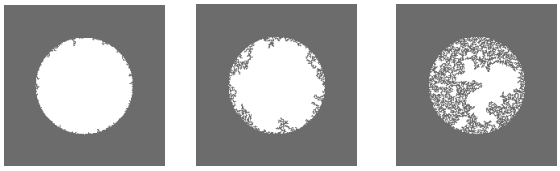

a) $p = 0.12$ *b)* $p = 0.51$ *c)* $p = 0.79$

Figure 5. The pore's over-time erosion

The structure formed in the manner described above we will call as a visual model of the membrane's surface.

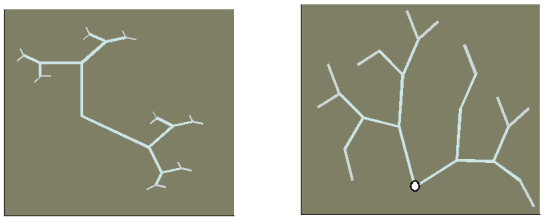

a) *b)*

Figure 6. The propagation of the crack

a) $H = 0.15$ *b)* $H = 0.5$ *c)* $H = 0.95$

Figure 7. The background of the membrane

The research problem of this paper can be formulated as follows:

can we find and classify the damages on the membrane's surface using its visual model and some methods of AI?

As it is possible to notice the responses to the research problem require some specific methodology. In next section, we will focus our attention on it.

3. RESEARCH METHODOLOGY

3.1. Method overview

It is obvious that, visual analysis of the membranes' surface condition requires special equipment that is better than the human eye can determine the place and character of the damage. In addition, in the expertise of the building structure, characterized as large areas, "manual" recognition of the pathologies' localization and classification is extremely time-consuming and often error-prone. Therefore, to solve the above problem, it would be helpful to have both a high-performance embedded device and a computational algorithm capable to complete real-time analysis of visual flow information. In such a manner the human factor can be eliminated for better performance and efficiency. In this study, we concentrate our attention only on the computational aspects.

Being a part of artificial intelligence, machine learning is widely used in image analysis. The advantage is due to the ability to come up with rules based on automated statistical processing of available data called training, that is to say mapping inputs (initial visual information) to associated targets or predictions (detected and classified defects). The remarkable progress made in this area can serve as a ruled defect-type classification by means of deep learning strategy, which includes:

- preprocessing (to speed up the recognition and the classification of the damages by normalizing and removing variations of initial visual information [10**]**);
- segmentation (to locate pores of the membrane and to detect desired features, i.e. their edges, using simplifications and changes in the representation of the pre-processed visual information avoiding as much as possible the problems initial data artifacts [11]);
- classification (to classify the extracted features into predefined categories by using

suitable methods that compare the image pattern with the predefined etalons [6]);
- post-processing (to correct errors caused by "oversegmentation" and "undersegmentation" and to improve the plausibility of the results [10, 11]);
- evaluation (to estimate the quality of previous steps [12]).

The choice of configuration of the deep learning algorithm depends on many factors associated with the available data, the purpose of their processing, as well as hardware and software.
Let us discuss these aspects in details.

3.2. Dataset

The membrane's surfaces were obtained by the simulation techniques described in subsection 2.2. The major advantage of artificially generated data is the availability of high-quality labeled training datasets for supervised, semi-supervised, and unsupervised deep learning used for object detection and recognition. The image dataset considered in this study is composed of 1000 same-size images. Each image contains 100 pores imitating the corruption processes. The lessons were automatically marked by pre-selection procedure with respect to the critical damage level $\tilde{p}$ and to the critical pore's radius value $\tilde{r} >> r_\ell(t_0)$, $\ell \in \mathcal{L}$, as well as automatically analyzed by the proposed methodology.

3.3. Image recognition: basic technique

3.3.1. Preprocessing. In the general case, the image preprocessing is applied to the original image and consists of the image resizing with further normalization and equalization as well as gamma correction pixels' intensities. Since we have assumed that $\mathcal{I}$ is the digital grayscale image generated as it was described in the subsection 2.2, we can omit the resizing procedure and the gamma-correction which allows the compensation for the non-linear luminance effect of optic devices. In this methodological approach we only need the normalization and the histogram equalization.

Consider the normalization step first. Keep in mind that the normalization is a kind of transformation applied to intensities of each pixel. Recall that the set of intensities of the initial image $\mathcal{I}$ was the set $\mathcal{F}$. The new values of intensities will be elements of the ordered final set $\tilde{\mathcal{F}}$ defined as

$$\tilde{\mathcal{F}} = \left\{ \tilde{f}_{\min}, ..., \tilde{f}_{\max} \right\},$$

where

$$\tilde{f}_{(x,y)} = \left(f_{(x,y)} - f_{\min} \right) \frac{\tilde{f}_{\max} - \tilde{f}_{\min}}{f_{\max} - f_{\min}} + \tilde{f}_{\min} . \quad (7)$$

For convenience, $\tilde{\mathcal{F}}$ can be rewritten with respect to the L-leveled gray scale in the following way

$$\tilde{\mathcal{F}} = \left\{ \tilde{f}_{\min} = \tilde{f}_0, ..., \tilde{f}_k, ..., \tilde{f}_{L-1} = \tilde{f}_{\max} \right\}. \quad (8)$$

Thus, we define a new image $\tilde{\mathcal{I}}$:

$$\tilde{\mathcal{I}} \underset{normalization}{\leftarrow} \mathcal{I} . \quad (9)$$

The goal of (7) is to enhance the contrast by redistributing the intensities toward extreme values. We insist on the fact that the image $\mathcal{I}$ contains also $n \times m$ pixels with the corresponding set of the intensities defined in (8).

Consider the histogram equalization step now. It is completed to normalize the gray color distribution across samples of images (mostly due to illumination, optics of devices etc.), that is to say the transformation of $\tilde{\mathcal{I}}$ into the new image $\tilde{\tilde{\mathcal{I}}}$. Therefore, let us introduce the quantities $\mathbb{T}\left(\tilde{f}_k\right)$, $0 \le k \le L-1$, such that

$$\mathbb{T}\left(\tilde{f}_k\right) = \sum_{\ell=0}^{k} \frac{m_\ell}{n\,m}, \quad (10)$$

where m_ℓ is the frequency of gray level ℓ. Here, we focus our attention on the frequentist probability. However, the other choice is also possible [10]. Next, we define

$$g\left(\tilde{f}_k\right)=\tilde{f}_{\min}+\left(\tilde{f}_{\max}-\tilde{f}_{\min}\right)\mathbb{T}\left(\tilde{f}_k\right), \quad (11)$$

and, hence, the set of intensities

$$\tilde{\tilde{\mathcal{F}}}=\left\{g\left(\tilde{f}_k\right),\ 0\le k\le L-1\right\}.$$

Thus, we get the new image

$$\tilde{\tilde{\mathcal{I}}} \underset{equalization}{\leftarrow} \tilde{\mathcal{I}}\ . \quad (12)$$

We also insist here, that $\tilde{\tilde{\mathcal{I}}}$ is the $n\times m$-pixels image with the set of intensities being $\tilde{\tilde{\mathcal{F}}}$.

3.3.2. Segmentation. The purpose of this step is to form homogeneous groups of pixels that could serve to assign them to the K specific objects $\bar{\omega}_\tau$, $1\le\tau\le K$ (usually a quantity of $\bar{\omega}_\tau$ are unknown before the segmentation). These elements form a subset $\bar{\Omega}=\left\{\bar{\omega}_\tau,\ 1\le\tau\le K\right\}$ of $\mathcal{D}$. The segmentation can be done by several techniques, namely: pixel-, edge-, region-, or model-based-techniques as well as the box-counting method. Taking into account the strengths and the weaknesses of these methods [Tosta], we search for the edges of pores by the modified Canny edge detector algorithm [Canny]. The main idea of this algorithm is as follows and consists in four phases.

Let $\mathbf{F}^*$ be a $n\times m$ matrix, such that the element of this matrix $f_{ij}^*\in\tilde{\tilde{\mathcal{F}}}$, $i\in\{1,...,n\}$, $j\in\{1,...,m\}$. The edge of each element of $\bar{\Omega}$ is determined by the transformation and the comparison of the intensities f_{ij}^* of neighboring pixels. In 2D image processing, two spatial variables θ_1 and θ_1 are related to $\mathbf{F}^*$. We denote the non-integer row index by θ_1 and the non-integer column index by θ_2.

Phase 1. Smoothing. The kernel regression filter takes a form

$$g\left(\theta_1,\theta_2\right)=\sum_{i=[\theta_1-3\sigma]}^{i=[\theta_1+3\sigma]}\sum_{j=[\theta_2-3\sigma]}^{j=[\theta_2+3\sigma]}\frac{f_{ij}^*}{2\pi\sigma^2}\exp\left(-\frac{(i-\theta_1)^2+(j-\theta_2)^2}{2\sigma^2}\right),$$

where σ is a smoothing parameter, which can be calculated as a standard deviation of pixel intensities of $\tilde{\tilde{\mathcal{I}}}$ or chosen arbitrary. It is used to avoid false detection and to riddle out the noise). Once applied to the image $\tilde{\tilde{\mathcal{I}}}$ this filter gives

$$\tilde{\tilde{\mathcal{I}}}^* \underset{\text{kernel regression}}{\leftarrow} \tilde{\tilde{\mathcal{I}}}. \quad (13)$$

Phase 2. Masking. To detect the black-white boundaries and in a consequence to determine edges of each element of $\bar{\Omega}$, firstly, the Laplacian

$$\mathbb{L}\left(g\left(\theta_1,\theta_2\right)\right)=\frac{\partial^2 g\left(\theta_1,\theta_2\right)}{\partial\theta_1^2}+\frac{\partial^2 g\left(\theta_1,\theta_2\right)}{\partial\theta_2^2} \quad (14)$$

is calculated, and, secondly, the mask $\mathbf{M}$ is the $n\times m$ matrix formed as

$$m_{\theta_1,\theta_2}=\begin{cases}0, & \ell_{\theta_1,\theta_2}<0,\\ 1, & \ell_{\theta_1,\theta_2}\ge 0,\end{cases} \quad (15)$$

where ℓ_{θ_1,θ_2} is the element of $\mathbb{L}\left(g\left(\theta_1,\theta_2\right)\right)$. In other words, zero-crossings in the Laplacian detect the white-black contours of each element of $\bar{\Omega}$.

Phase 3. Hysteresis. The Richardson extrapolation is applied to values of the $n\times m$ matrix $\mathbf{M}$. This permits to finalize the detection of edges of each element of $\bar{\Omega}$ by suppressing all the other edges that are not connected to strong edges.

Phase 4. Morphology and boundary statistics. The application of the Fourier descriptor allows

finding the boundaries as well as calculate the area of each strong edge $\bar{\omega}$.
To conclude the segmentation step, the set $\bar{\Omega}$ contains K elements $\bar{\omega}$, each one $\bar{\omega}$ is defined by two parameters, namely: the contour $\mathcal{C}_{\bar{\omega}}$ and the area $\mathcal{A}_{\bar{\omega}}$.

3.3.3. Classification. Once being detected the elements $\bar{\omega} \in \bar{\Omega}$ can be classified either like corrupted pores (if the radius r exceeds the critical value $\tilde{r}$ and if the surface corruption parameter p exceeds the critical value $\tilde{p}$) or like non-corrupted ones. The sets of corrupted and non-corrupted pores are $\bar{\Omega}_{-1}$ and $\bar{\Omega}_{+1}$, correspondently,

$$\bar{\Omega}_{-1} \bigcap \bar{\Omega}_{+1} = \varnothing$$

and

$$\bar{\Omega}_{-1} \bigcup \bar{\Omega}_{+1} = \bar{\Omega}.$$

The patterns of the pores are defined by the formula (2). We denote them by $\omega \in \Omega$, each contour $\mathcal{C}_{\omega}$ of ω corresponds to the border of $\mathcal{R}_{\ell}(t_1)$ and $\mathcal{A}_{\omega} = \pi r_{\ell}^2(t_1)$, $\ell \in \mathcal{L}$. We also introduce the set of labels $\Xi = \{-1, 1\}$ such that each element $\xi \in \Xi$ is given by

$$\xi_{\ell} = \begin{cases} -1, & for\ \ r_{\ell}(t_1) < \tilde{r}\ \ and\ \ p_{\ell} < \tilde{p}, \\ +1, & for\ \ r_{\ell}(t_1) \geq \tilde{r}\ \ or\ \ p_{\ell} \geq \tilde{p}, \end{cases}$$

thus, if $\xi_{\ell} = -1$, then $\omega_{\ell} \in \Omega_{-1}$, and if $\xi_{\ell} = +1$, then $\omega_{\ell} \in \Omega_{+1}$, moreover, $\Omega_{-1} \bigcap \Omega_{+1} = \varnothing$ and $\Omega_{-1} \bigcup \Omega_{+1} = \Omega$.
The classification problem can be formulated as follows:
for a training set of pairs $\{\omega_{\ell}, \xi_{\ell}\}_{\ell=1}^{\mathcal{L}}$, *where* ω_{ℓ} *are input patterns from the set of patterns* Ω *and* $\xi_{\ell} \in \Xi$ *are the corresponding labels, find a classifier* $\eta(\bar{\omega})$ *such that to get as few errors as possible.*
Let us introduce the classifier

$$\eta(\omega_{\ell}, \bar{\omega}) = \sum_{\ell \in \mathcal{L}} \alpha_{\ell} \xi_{\ell} \mathrm{K}(\omega_{\ell}, \bar{\omega}) + b, \quad (15)$$

where K is a kernel, $b \in \mathbb{R}$ is a shift, the parameters $\alpha_{\ell} \in \mathbb{R}$ form a weight vector $\boldsymbol{\alpha}$ of the training element ω_{ℓ}. We put

$$\|\boldsymbol{\alpha}\|_0 = \sum_{\ell \in \mathcal{L}} \mathbf{1}_{\{\alpha_{\ell} \neq 0\}} \quad (16a)$$

and

$$\|\boldsymbol{\alpha}\|_1 = \sum_{\ell \in \mathcal{L}} |\alpha_{\ell}|. \quad (16b)$$

Therefore, the goal is to solve the non-convex discontinuous optimization problem

$$\arg\min_{\boldsymbol{\alpha}} \left\{ \|\boldsymbol{\alpha}\|_0 + C \sum_{\ell \in \mathcal{L}} \phi(\xi_{\ell} \eta(\omega_{\ell}, \bar{\omega})) \right\} \quad (17)$$

$$\text{s.t. } 0 \leq \|\boldsymbol{\alpha}\|_1 \leq C, \quad (18)$$

where C is a hyperparameter and

$$\phi(z) = \begin{cases} 1 - z, & z \leq 1, \\ 0, & z > 1 \end{cases} \quad (19)$$

is the hinge loss. Here, we admit that the solution of the problem (17) - (19) can be found by standard procedure included to ALADIN Optimization ToolBox MatLab [14].

Post-processing. To evaluate the segmentation and classification stages we use the following idea. We suppose that a reference image contains k_1 regions (it can be generated by the procedure described in section 2.2 such that $k_1 = n_x \times n_y$) and k_2 regions detected by the segmentation or by the classification proce-

dures. Let A_i be the i^{th} region on a reference image demarcated by a specialist and B_j be the j^{th} corresponding segmented image ($i \in \{1,2,...,k_1\}$, $j \in \{1,2,...,k_2\}$). It is clear that in both cases regions contain pixels, therefore we treat any region as a set. In an ideal situation $k_1 = k_2$ and $A_i = B_i$ for any $i \in \{1,2,...,k_1\}$. This situation is extremely rare. In practice the following situations are possible:

- $k_1 = k_2$ – the algorithm found the same number of regions, the sets A_i and B_i cover approximately the same domain for any $i \in \{1,2,...,k_1\}$ (see Fig. 8);
- $k_1 > k_2$ – the algorithm found fewer regions than it was marked, for any $i \in \{1,2,...,k_2\}$ the sets A_i and B_i cover approximately the same domain and for any $j \in \{k_2+1,...,k_1\}$ $B_j = \varnothing$;
- $k_1 < k_2$ – the algorithm found more regions than it was marked, for any $i \in \{1,2,...,k_1\}$ the sets A_i and B_i cover approximately the same domain and for $i \in \{k_1+1,...,k_2\}$ $A_i = \varnothing$.

When two the sets A and B cover approximately the same domain, it implies that the sets A and B are not disjoint and than A is a strict subset of $A \bigcup B$. Based on this remark, we can propose the following evaluation criteria (called by us "the domain of confidence criteria" - DoC), defined as follows

$$DoC := \sum_{i=1}^{min\{k_1,k_2\}} \frac{\mathbb{P}(A_i \bigcap B_i)}{\mathbb{P}(A_i)}, \qquad (20)$$

$$DoC \geq \beta \frac{\min\{k_1,k_2\}}{\max\{k_1,k_2\}}, \qquad (21)$$

where $\beta \in (0,1)$ is a resemblance parameter, which has to be carefully chosen (or estimated). The notation $\mathbb{P}$ denotes once the area of the set, which is used for the segmentation procedure, and once the number of pixels, defined by the classification procedure.

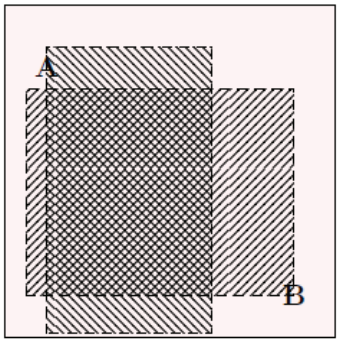

Figure 8. Relation between region A identified by an expert and region B identified by computational techniques.

4. RESULTS AND DISCUSSION

To detect and to classify the damages on the membrane surface, five categories of membrane surface were defined mainly due to differentiation of their backgrounds. The backgrounds were simulated as fractional Brownian fields with five different values of Hurst parameter

$$H \in \{0.05, 0.25, 0.50, 0.75, 0.95\}.$$

Each category contained 200 gray-scale images. The gray scale used 256 different intensities. Each 120×120-pixels-image was full of 100 pores distributed in equidistant–grid nodes. The pixel intensities of each pore's edge were coded by 120, the micro-cracks pixel and crack propagation intensities were coded by 80 and 160 correspondently. The pores evolution was done by 100 steps on the time interval $[0,1]$. The initial radius value for each one pore was $r_\ell(t_0) = 2$, the new radius value was randomly selected from the interval $[2,5]$, the critical value was $\tilde{r} = 4$. The corruption level was increasing by each evolutionary step by randomly selected value from the interval $[0, 0.05]$, the crit-

ical damage level was $\tilde{p} = 0.7$. All these images were divided on the training and evolution sets as "3:1". The segmentation and classification procedures were developed using convolutional neural networks (ConvNets, CNNs) included in Deep Learning Toolbox MatLab R2020a. Once the training was done, the image recognition was done for 100 generated surfaces with different values of H. The averaged statistics of the numerical experiments are listed in Tables 1–3, k_1 stands for the number of corrupted pores after the evolution.

Let us comment on the results. Initially, all the objects of interest are homogeneous. However, evolution makes them non-homogeneous. The backgrounds of the membrane's surface, as well as corrupted pores, contain fractional noises, which restrict the effectiveness of segmentation by the intensity-threshold-based method. The influence of a smoothing parameter σ in global senses on the quality of the problem-solution was studied in the first series of experiments (see Table 1). As it was possible to expect, the inhomogeneous backgrounds ($H = 0.05$ and $H = 0.25$) provoke more erroneous detections of corrupted pores then that in the case of $H \geq 0.5$. With increase of σ improves the both statistics (20) and (21). The local smoothing works better then the global one (see Table 2 and Table 3). We can observe the improvement of DoC statistics for highly noisy conditions.

Table 1. Simulation results with the predefined smoothing parameter of kernel regression

H	σ	$\overline{DoC}$	$\lceil \bar{k}_1 \rceil$	$\lceil \bar{k}_2 \rceil$	$\bar{\beta}$
0.05	1	0.5311	51	63	0.4299
0.25	1	0.5492	49	41	0.6563
0.50	1	0.8002	55	57	0.8292
0.75	1	0.6724	56	52	0.7241
0.95	1	0.7310	60	55	0.7975
0.05	2	0.5663	47	56	0.6747
0.25	2	0.5715	52	43	0.6911
0.50	2	0.8533	49	46	0.9090
0.75	2	0.7893	54	49	0.8698
0.95	2	0.8884	52	49	0.9427
0.05	3	0.5718	53	62	0.6689
0.25	3	0.5794	54	47	0.6657
0.50	3	0.8807	48	50	0.8455
0.75	3	0.7956	61	58	0.8368
0.95	3	0.8582	54	51	0.9087

Table 2. Simulation results with the estimated on 5×5 pixel neighborhood smoothing parameter of kernel regression

H	$\overline{DoC}$	$\lceil \bar{k}_1 \rceil$	$\lceil \bar{k}_2 \rceil$	$\bar{\beta}$
0.05	0.6200	56	49	0.7086
0.25	0.6587	48	51	0.6999
0.50	0.8338	58	54	0.8956
0.75	0.8105	57	62	0.8816
0.95	0.8453	61	57	0.9046

However, in all cases, the results still showed incorrect identification of corrupted pores or by their quantity or by their surface. It can be explained by the weak performance of the normalization procedure, which has to be adapted to highly noisy backgrounds and more careful selection of the optimization procedure for the solution of (17)–(18).

Table 3. Simulation results with the estimated on 7×7 pixel neighborhood smoothing parameter of kernel regression

H	$\overline{DoC}$	$\lceil \bar{k}_1 \rceil$	$\lceil \bar{k}_2 \rceil$	$\bar{\beta}$
0.05	0.7225	52	47	0.7993
0.25	0.7199	61	58	0.7571
0.50	0.8401	55	53	0.8718
0.75	0.8539	47	45	0.8156
0.95	0.8600	54	51	0.9105

5. CONCLUSIONS

This study presented the computational strategy for the detection of the membrane's defected recognitions. Its main advantage is due to a multi-agent simulation of the object of interest be-

havior. Once having values of physical, chemical, or mechanical parameters of water-proofing materials, we can develop different scenarios to predict the material performance. The effective results depend on the careful selection of the parameters of the method's sequential steps. One limitation of the proposed method is the quantity of false detected regions, which is a common phenomenon for highly noisy backgrounds of images [12, 13]. To make this methodology helpful for object detection in different fields of interests such as civil engineering, biology, medicine, or forensic science, we should consider non-Gaussian filters concerning the spatial distribution of image intensities and perform complex analysis of the algorithm.

REFERENCES

1. **Cui H., Li Y., Zhao X., Yin X., Yu J., Ding B.,** Multilevel porous structured polyvinylidene fluoride/polyurethane fibrous membranes for ultrahigh waterproof and breathable application. // Composites Communications, 2017, Volume 6, pp. 63-67.
2. **Lee K., Kim D., Chang S.-H., Choi S.-W., Park B., Lee C.**, Numerical approach to assessing the contact characteristics of a polymer-based waterproof membrane. // Tunnelling and Underground Space Technology, 2018, Volume 79, pp. 242-249.
3. **Rupal A., Sharma S.K., Tyagi G.D.**, Experimental investigation on mechanical properties of polyurethane modified bituminous waterproofing membrane. // Materials Today: Proceedings, 2019.
4. **Walter A., de Brito J., Grandão Lopes J.**, Current flat roof bituminous membranes waterproofing systems – inspection, diagnosis and pathology classification. // Construction and Building Materials, 2005, Volume 19 (3), pp. 233-242.
5. **Yin F., Hu P., Song C., Wang S., Liu H.**, Unveiling the role of gas permeability in air cathodes and performance enhancement by waterproof membrane fabricating method. // Journal of Power Sources, 2020, Volume 449, pp. 227570.
6. **Song Y., Huang Z., Shen Ch., Humphrey Shi, Lange D.A.**, Deep learning-based automated image segmentation for concrete petrographic analysis. // Cement and Concrete Research, 2020, Volume 135, 106118.
7. **Pathan A. K., Monowar M.M., Khan S**. Simulation Technologies in Networking and Communications: Selecting the Best Tool for the Test. CRC Press, 2015
8. **Kroese D. P., Botev Z. I.** Spatial Process Simulation. // Stochastic Geometry, Spatial Statistics and Random Fields Springer International Publishing, 2015, pp. 369-404.
9. **El-Nouty C.**, On approximately stationary Gaussian processes // International Journal for Computational Civil and Structural Engineering, 2015, Volume 11, Issue, pp. 15-26.
10. **Ramírez-Gallego S., Krawczyk B., García S., Woźniak M., Herrera F.** A survey on data preprocessing for data stream mining: Current status and future directions. // Neurocomputing, 2017, Volume 239, pp. 39-57.
11. **Lou Q., Peng J., Wu F., Kong D.** Variational Model for Image Segmentation. In: Bebis G. et al. (eds) Advances in Visual Computing. ISVC 2013. Lecture Notes in Computer Science, Volume 8034, 2013, Springer, Berlin, Heidelberg.
12. **Ma T., Antoniou C., Toledo T**. Hybrid machine learning algorithm and statistical time series model for network-wide traffic forecast. // Transportation Research Part C: Emerging Technologies, 2020, Volume 111, pp. 352-372.
13. **Tosta T., Faria P.R. , Alves Neves L , Zanchetta do Nascimento M.** Computational method for unsupervised segmentation of lymphoma histological images based on fuzzy 3-partition entropy and genetic algorithm. // Expert Systems with Applications, 2017, Volume 81, pp. 223-243.
14. **Engelmann A., Jiang Y., Muhlpfordt T.,**

Houska B., Faulwasser T., Toward distributed OPF using ALADIN. // IEEE Transactions on Power Systems, 2019, Volume 34 (1), pp. 584-594.

СПИСОК ЛИТЕРАТУРЫ

1. **Cui H., Li Y., Zhao X., Yin X., Yu J., Ding B.,** Multilevel porous structured polyvinylidene fluoride/polyurethane fibrous membranes for ultrahigh waterproof and breathable application. // Composites Communications, 2017, Volume 6, pp. 63-67.
2. **Lee K., Kim D., Chang S.-H., Choi S.-W., Park B., Lee C.**, Numerical approach to assessing the contact characteristics of a polymer-based waterproof membrane. // Tunnelling and Underground Space Technology, 2018, Volume 79, pp. 242-249.
3. **Rupal A., Sharma S.K., Tyagi G.D.**, Experimental investigation on mechanical properties of polyurethane modified bituminous waterproofing membrane. // Materials Today: Proceedings, 2019.
4. **Walter A., de Brito J., Grandão Lopes J.**, Current flat roof bituminous membranes waterproofing systems – inspection, diagnosis and pathology classification. // Construction and Building Materials, 2005, Volume 19 (3), pp. 233-242.
5. **Yin F., Hu P., Song C., Wang S., Liu H.**, Unveiling the role of gas permeability in air cathodes and performance enhancement by waterproof membrane fabricating method. // Journal of Power Sources, 2020, Volume 449, pp. 227570.
6. **Song Y., Huang Z., Shen Ch., Humphrey Shi, Lange D.A.**, Deep learning-based automated image segmentation for concrete petrographic analysis. // Cement and Concrete Research, 2020, Volume 135, 106118.
7. **Pathan A. K., Monowar M.M., Khan S**. Simulation Technologies in Networking and Communications: Selecting the Best Tool for the Test. CRC Press, 2015
8. **Kroese D. P., Botev Z. I.** Spatial Process Simulation. // Stochastic Geometry, Spatial Statistics and Random Fields Springer International Publishing, 2015, pp. 369-404.
9. **El-Nouty C.**, On approximately stationary Gaussian processes // International Journal for Computational Civil and Structural Engineering, 2015, Volume 11, Issue, pp. 15-26.
10. **Ramírez-Gallego S., Krawczyk B., García S., Woźniak M., Herrera F.** A survey on data preprocessing for data stream mining: Current status and future directions. // Neurocomputing, 2017, Volume 239, pp. 39-57.
11. **Lou Q., Peng J., Wu F., Kong D.** Variational Model for Image Segmentation. In: Bebis G. et al. (eds) Advances in Visual Computing. ISVC 2013. Lecture Notes in Computer Science, Volume 8034, 2013, Springer, Berlin, Heidelberg.
12. **Ma T., Antoniou C., Toledo T**. Hybrid machine learning algorithm and statistical time series model for network-wide traffic forecast. // Transportation Research Part C: Emerging Technologies, 2020, Volume 111, pp. 352-372.
13. **Tosta T., Faria P.R. , Alves Neves L , Zanchetta do Nascimento M.** Computational method for unsupervised segmentation of lymphoma histological images based on fuzzy 3-partition entropy and genetic algorithm. // Expert Systems with Applications, 2017, Volume 81, pp. 223-243.
14. **Engelmann A., Jiang Y., Muhlpfordt T., Houska B., Faulwasser T.**, Toward distributed OPF using ALADIN. // IEEE Transactions on Power Systems, 2019, Volume 34 (1), pp. 584-594.

Филатова Дарья, профессор, доктор физико-математических наук работает на кафедре информатики факультета Компьютерных систем и сетей Белорусского Государственного Университета Информатики и Радиоэлектроники, Минск, Беларусь и в лаборатории Человеческого и искусственного интеллекта Практическая Школа Высших Исследований , 4–14 ул. Ферруса, 75014 Париж, Франция;

E-mail: filatova@bsuir.by;
orcid.org/0000-0001-9434-7993.

Professor, Dr. hab. Darya Filatova works in Informatics Department, Faculty of Computer Systems and Networks, Belarusian State University of Informatics and Radioelectronics, and CHART EPHE, 4-14 Rue Ferrus, 75014 Paris, France; e-mail: filatova@bsuir.by;
orcid.org/0000-0001-9434-7993.

Шарль Эль-Нути – профессор, доктор физико-математических наук работает в лаборатории ЛАГА, Университет Сорбонна Париж Север; авенью Ж.-Б. Кленанта, д. 99, 94340 Вильтанез, Франция;
E-mail: elnouty@math.univ-paris13.fr,
orcid.org/0000-0002-2321-1041

Professor, Dr. hab. Charles El-Nouty works in LAGA, Université Sorbonne Paris Nord; 99 avenue J-B Clément 93430 Villetaneuse;
E-mail: elnouty@math.univ-paris13.fr;
orcid.org/ /0000-0002-2321-1041

Владислав Валерьевич Пунько является студентом магистрантом кафедре информатики факультета Компьютерных систем и сетей Белорусского Государственного Университета Информатики и Радиоэлектроники, Минск, Беларусь; 220013, Республика Беларусь, г. Минск, ул. Гикало, д. 9;
E-mail: iam.vlad.punko@gmail.com;
orcid.org/0000-0002-2947-3245

Uladzislau Valerevich Punko is a master's student of Informatics Department, Faculty of Computer Systems and Networks, Belarusian State University of Informatics and Radioelectronics, Gikalo 9, 220005 Minsk, Belarus;
E-mail: iam.vlad.punko@gmail.com;
orcid.org/ 0000-0002-2947-3245